Atmos. Chem. Phys. Discuss., 15, 1523–1571, 2015
www.atmos-chem-phys-discuss.net/15/1523/2015/
doi:10.5194/acpd-15-1523-2015

Atmospheric Chemistry and Physics Discussions

The climatology of dust aerosol over the arabian peninsula

A. Shalaby[1], **B. Rappenglueck**[2], **and E. A. B. Eltahir**[3]

[1]The International Centre for Theoretical Physics, Trieste, Italy
[2]Department of Earth and Atmospheric Sciences, University of Houston, Texas 77004, USA
[3]Massachusetts Institute of Technology, Cambridge, Massachusetts, USA

Received: 25 September 2014 – Accepted: 19 December 2014 – Published: 19 January 2015

Correspondence to: A. Shalaby (ashalaby@ictp.it)

Published by Copernicus Publications on behalf of the European Geosciences Union.

Abstract

Dust storms are considered to be a natural hazard over the Arabian Peninsula, since they occur all year round with maximum intensity and frequency in Spring and Summer. The Regional Climate Model version 4 (RegCM4) has been used to study the climatology of atmospheric dust over the Arabian Peninsula from 1999 to 2012. This relatively long simulation period samples the meteorological conditions that determine the climatology of mineral dust aerosols over the Arabian Peninsula. The modeled Aerosol Optical Depth (AOD) has been compared against ground-based observations of three Aerosol Robotic Network (AERONET) stations that are distributed over the Arabian Peninsula and daily space based observations from the Multi-angle Imaging SpectroRadiometer (MISR), the Moderate resolution Imaging SpectroRadimeter (MODIS) and Ozone Monitoring Instrument (OMI). The large scale atmospheric circulation and the land surface response that lead to dust uplifting have been analyzed. While the modeled AOD shows that the dust season extends from March to August with two pronounced maxima, one over the northern Arabian Peninsula in March with AOD equal to 0.4 and one over the southern Arabian Peninsula in July with AOD equal to 0.7, the observations show that the dust season extends from April to August with two pronounced maxima, one over the northern Arabian Peninsula in April with AOD equal to 0.5 and one over the southern Arabian Peninsula in July with AOD equal to 0.5. In spring a high pressure dominates the Arabian Peninsula and is responsible for advecting dust from southern and western part of the Arabian Peninsula to northern and eastern part of the Peninsula. Also, fast developed cyclones in northern Arabian Peninsula are responsible for producing strong dust storms over Iraq and Kuwait. However, in summer the main driver of the surface dust emission is the strong northerly wind ("Shamal") that transport dust from the northern Arabian Peninsula toward south parallel to the Arabian Gulf. The AERONET shortwave Top of Atmosphere Radiative Forcing (TOARF) and at the Bottom of Atmosphere Radiative Forcing (BOARF) have been analyzed and compared with the modeled direct radiative forcing of mineral dust aerosol. The annual

ACPD
15, 1523–1571, 2015

modeled TOARF and BOARF are −3.3 and −12 W m^{-2}, respectively. However, the annual observed TOARF and BOARF are significantly different at −10 and −52 W m^{-2}, respectively. The analysis of observed and modeled TOARF agrees with previous studies in highlighting the need for more accurate specification of surface albedo over the region. Due to the high surface albedo of the central Arabian Peninsula, mineral dust aerosols tend to warm the atmosphere in summer (June–August).

1 Introduction

Atmospheric mineral dust is a natural aerosol and is ubiquitous in the Earth's atmosphere, despite that it is emitted from hyper-arid, arid and semi-arid regions on the globe. About 2000 Mt is emitted annually to the atmosphere, 1500 Mt is deposited to the land and 500 Mt is deposited onto the ocean surface (Shao et al., 2011). It affects radiation by absorption and scattering that in turn affects surface and atmospheric temperature, also it acts as ice cloud condensation nuclei (ICCN) that impacts the microphysics of the clouds and its radiative properties (IPCC, 2013). The transported dust also carries nutrients and bacteria, which may affect the marine life and land surface life. For instance, 20 Mt of nutrients rich Saharan dust is transported to the Amazon basin in South America each year (Koren et al., 2006). Atmospheric mineral dust, especially fine dust (smaller than 2.5 µm) may cause cardiopulmonary disease and lung cancer (Giannadaki et al., 2014). It also affects many of human activities like aviation, real estate construction, agriculture, and water resource management (Stefanski and Sivakumar, 2009).

Dust particles are emitted from major deserts on the globe (e.g., Sahara, the Arabian Peninsula, Taklamakan and Gobi deserts in China, Australia deserts and Atacama desert in Chile). The mineral dust emission processes (i.e., saltation and sandblasting) are determined by meteorological conditions (e.g., atmospheric instability, soil moisture). Large-scale wind systems may carry coarse and fine dust particles horizontally for thousands of kilometers (e.g., Koren et al., 2006) and vertically up 6 to 10 km (e.g.,

ACPD
15, 1523–1571, 2015

Gobbi et al., 2004). Depending on dust particle size and atmospheric conditions dust particles may remain airborne between 1.5 to 7.4 days and will then deposit to the surface by gravitational settling or rain washout (Shao et al., 2011).

This paper focuses on atmospheric mineral dust over the Arabian Peninsula, a region, which has been less studied over the last decades compared to Saharan regions.

In an early study Wilkerson (1991) described the onset and evolution of dust storms over Iraq and Kuwait analyzing satellite images and visbility records. Wilkerson's study categorized the types of dust storms as pre-frontal, post-frontal and Shamal types, the latter being a regional northwesterly wind that typically occurs in summer ("Shamal" denotes "northerly wind" in Arabic). Mashat et al. (2008) used meteorological observations from Saudi Arabia to analyze the meteorological conditions which favored dust storms and their spatial and seasonal distribution. They found that dust storms most frequently occur in the eastern part of the Arabian Peninsula in spring and extend towards the southern part of the Arabian Peninsula in summer. Alharbi (2009) and Alharbi et al. (2013) explored dust storms generation over the Arabian Peninsula, dust source regions and atmospheric conditions that promote dust storms, which include large-scale atmospheric instability, high surface winds, and dry, rich dust sources. The quantification and characterization of mineral dust aerosol (e.g., dust concentrations profile and mineral dust optical properties) became possible after the installation of The **AE**rosol **RO**botic **NET**work (AERONET) in Bahrain and Saudi Arabia around 1998. Smirnov et al. (2002) used a one year data record (July 1998–July 1999) of the Bahrain site in the Arabian Gulf to deduce the climatology of aerosol optical properties (i.e., the Aerosol Optical Depth (AOD) and the Ångström parameter). In 2004 an intensive measurement campaign was held in the United Arab Emirates (UAE), which led to the installation of various AERONET stations. Among them only the Mezaira site is fully operational up to date. This campaign characterized the nature of atmospheric aerosol over the UAE and validated satellite aerosol products over a bright surface such as desert (Reid et al., 2005; Eck et al., 2008). Kim et al. (2011) studied AERONET data records from North Africa and the Arabian Peninsula and derived the seasonal behav-

ACPD
15, 1523–1571, 2015

ior of mineral dust aerosol optical properties in these regions. This study showed that the Arabian Peninsula dust is more absorbing in the shortwave range than the Saharan dust does. García et al. (2012) analyzed most of the AERONET stations on the globe including the Arabian Peninsula and found that atmospheric aerosols over high surface albedo regions, as deserts, lead to a warming of the Earth's atmosphere.

Using a regional climate model offers the advantage to investigate meso-scale phenomena such as surface dust emission processes, transportation, deposition and its radiative impact on the regional climate at a higher spatial resolution (e.g., ≤ 50 km) than global models with coarse spatial resolution (e.g., ≥ 100 km). The Regional Climate Model Version 3 (RegCM3) (Pal et al., 2007) and RegCM4 (Giorgi et al., 2012) have been used to investigate mineral dust aerosols and its radiative impact on regions in North and West Africa (Zakey et al., 2006; Solmon, 2008; Konarè et al., 2008; Napat et al., 2012; Steiner et al., 2014), but studies on the Middle East area are rare. Marcella and Eltahir (2010, 2011) used RegCM3 for the first time over the Northern Arabian Peninsula, to explore the impact of dust on climate and found that the implementation of subgrid wind variability and dust aerosol lateral boundary conditions could enhance the dust simulation. Nazrul Islam and Almazroui (2012) used RegCM4, showed that the direct radiative effect of mineral dust results in a decrease of surface temperature and increase in precipitation over the Arabian Peninsula in the wet season (November–April).

The first objective of this study is to define and identify the dust season by means of available observations (e.g. through AERONET and satellite data bases) and regional climate modeling. As the uncertainties of aerosol radiative forcing are large (IPCC, 2013), more investigation on the sources of such uncertainties, especially on regional scales, is needed. Thus, the second objective of this study is to estimate the Bottom Of Atmosphere Radiative Forcing (BOARF) and the Top of Atmosphere Radiative Forcing (TOARF) of mineral dust aerosols using AERONET products and the model. These objectives integrate observations and modeling to obtain a better assessment of the atmospheric behavior of mineral dust aerosol.

ACPD
15, 1523–1571, 2015

2 Methods

2.1 Observational datasets

The observation of atmospheric dust from space has become very vital to the understanding of this phenomenon. Space-borne observations provide global information of the spatial distribution (horizontal and vertical) and the temporal evolution of the Aerosol Optical Depth (AOD). However, comparison of modeled dust (AOD) with satellite measurements may be problematic, since satellite observations apply assumptions about the nature of the aerosol, which is different from approaches in numerical models (Woodward, 2001). On the other hand, ground-based observation is needed to provide more details of atmospheric dust characteristics such as high frequency measurements of near ground concentration (e.g., PM10) and AOD. Also ground-based measurements include physical and chemical analysis of aerosols, such as its geometrical shape, size distribution and chemical composition. The ground-based measurements are also used to validate the space-borne observations. For instance, the AOD from AERONET stations has been used to validate satellite AOD products (Martonchik et al., 2004; Abdou et al., 2005). In the following subsections we will briefly discuss the characteristics of AERONET and satellite datasets.

2.1.1 AERONET

The **AE**rosol **RO**botic **NET**work (AERONET) provides valuable measurements of atmospheric aerosol optical properties. AERONET stations comprise an automatic sun photometer. It has its own algorithm to evaluate data quality and instrument functionality. AERONET measures AOD for different wavelengths, from near IR (1064 nm) to near UV (340 nm). AERONET sunphotometer provides information about aerosol size distribution, aerosol radiative forcing, and aerosol shape (spherical/non-spherical). Detailed description of the instrument and its function can be found in Holben et al. (1998).

ACPD
15, 1523–1571, 2015

The measurements pass multilevel quality assurance (QA): level 1 without cloud screening, level 1.5 has cloud screened but may be without final calibration. Level 2 has cloud screened and quality assured calibrations. The AOD accuracy of calibrated AERONET station is wavelength dependent and varies from root mean square error of ±0.012 (UV band) to root mean square error of ±0.006 (IR band) at overhead sun (airmass = 1) (Schmid et al., 1999).

The AERONET stations are widely used over the globe. However there are only few AERONET stations in the Arabian Peninsula with relatively long measurement records. Among them is the Solar-Village station in Saudi Arabia, the Kuwait University station in Kuwait and the Mezaira site in the United Arab Emirates (UAE). For detailed information about the site and their locations see Table 1 and Fig. 1.

Each station has its unique features; the Kuwait station is downwind of major dust sources in Southern Iraq. Solar-Village is located in the center of Saudi Arabia and it is at a relatively high altitude (764 m a.s.l.) compared to other sites, which could reflect the transportation of dust to high altitudes. Mezaira in United Arab Emirate (UAE) is inland site and could be considered a receptor site for dust coming from southern Arabian Peninsula.

2.1.2 MISR

Most satellite instruments looks down to the earth (0 degrees Nadir angle), or toward the edge of the planet and receive the reflected sunlight. The Earth's surface, clouds and aerosols reflect sunlight in different direction, which requires an instrument that accounts for such different reflected angle. The Multiangle Imaging Spectroradiometer (MISR) is a unique instrument flown in the space since late 1998. It has nine cameras corresponding to nine view angles, the middle one pointing toward the nadir, four of them in a forward direction with (26.1, 45.6, 60.0 and 70.0°, respectively) relative to the nadir camera and the other four in the rearward direction with (−26.1, −45.6, −60.0 and −70.0° respectively). Each direction measures four individual wavelength (443, 555, 670 and 865 nm). Therefore, MISR has 36 channels (Diner et al., 1998). MISR

ACPD
15, 1523–1571, 2015

has been used in many fields including studies on, clouds (Marchand et al., 2010), aerosols (Martonchik et al., 2004; Abdou et al., 2005; Marey et al., 2011) and Earth surface (Pinty et al., 2011). For our purpose, we will focus on the aerosol facilities of MISR. The MISR global aerosol retrieval is used to obtain AOD values to characterize the types of aerosol based on their physical and optical properties, and aerosol particle shape (spherical or non-spherical). The aerosol retrieval algorithm strategy has many steps. First, it utilizes a lookup table that contains a suite of a natural aerosol types and calculated aerosol optical properties by a radiative transfer model. Second, the retrieval of the aerosol over dark surfaces like the ocean depends on red and near infrared (IR) channels (Martonchik et al.,1998). The most difficult retrieval is above bright surface like deserts. This latter retrieval needs special treatment and is therefore associated with large uncertainties (Diner, 1998; Martonchik, 1998; Abdou et al., 2005).

In this work we concentrate only on the MISR AOD dataset and its comparison with the model output. The MISR data used in our study spans 6 years from 2006 to 2012. The data resolution is $0.5^{\circ} \times 0.5^{\circ}$. Data has been retrieved from the Giovanni website (http://Giovanni.gsfc.nasa.gov/giovanni).

2.1.3 MODIS (Deepblue)

The Moderate Resolution Imaging Spectroradiometer (MODIS) instrument is aboard the NASA EOS (Earth Observing System) Terra and Aqua satellites and began transmitting date in 2000. The instruments have high spatial resolution (10 km resolution) and almost global coverage. Like MISR, MODIS aerosol retrievals are based on a lookup table procedure in which the satellite measured radiances are matched to pre-calculated values in the lookup table. The values of the aerosol properties used to create the calculated radiances are retrieved (Remer et al., 2005; Abdou et al., 2005). The MODIS data set spans from January 2008 to December 2011. Data has been retrieved from the Giovanni website (http://Giovanni.gsfc.nasa.gov/giovanni).

ACPD
15, 1523–1571, 2015

2.1.4 OMI

The Ozone Monitoring Instrument (OMI) has been orbiting the Earth on one of the EOS mission "Aura spacecraft" since July 2004. OMI is a high spatial resolution (13 km × 24 km) ground pixel size ultraviolet/visible (UV/VIS) backscatter spectrometer (Levelt et al., 2006). The OMI aerosol retrieval algorithm is the same as for the Total Ozone Mapping spectrometer (TOMS) near-UV method of aerosol absorption sensing from space (Torres et al., 2005). The accuracy of the OMI retrieval of aerosol optical depth is around 30 % relative to AERONET measurements (Torres et al., 2005).

The extinction AOD at 500 nm (near-UV) has been selected from the OMI product from Giovanni site portal (http://Giovanni.gsfc.nasa.gov/giovanni). From that data we selected 2° × 2° box around the three AERONET stations (see Fig. 1) for comparison purposes with the observations. The time span of this data is from January 2008 to December 2011.

2.2 Model description and experimental design

2.2.1 General model description

The International Centre for Theoretical Physics (ICTP) Regional Climate Model (RegCM) was built upon the National Center for Atmospheric Research (NCAR) Mesoscale Model version 4 (MM4) (Giorgi and Bates, 1989; Giorgi et al., 1993a, b).

The Regional Climate Model version 4 (RegCM4) is the second major development of the RegCM core after RegCM3 (Pal et al., 2007). The coding structure is completely changed. It has become totally FORTRAN 90 compliant and modular structured and its parallelization and memory management has become more efficient. The RegCM4 has more physics options, which include the Community Land surface Model (CLM3.5) land surface parameterization, the Tiedtke convection scheme, the University of Washington (UW) planetary boundary layer (PBL) scheme, and the Rapid Radiative Transfer Model (RRTM) (Giorgi et al., 2012).

ACPD
15, 1523–1571, 2015

RegCM4 is an online climate-chemistry model and has an online gas-phase chemistry scheme (CBMZ) (Shalaby et al., 2012). It has various aerosol components such as, four size bin dust, two size bin sea salt, sulphate, black carbon and organic carbon. Sulphate, black carbon and organic carbon (Solmon et al., 2006), as well as dust and sea-salt are radiatively active (Zakey et al., 2006, 2008).

2.2.2 Dust parameterization

Sand particles are affected by many forces that determine their fate. Dust particles have three dynamic modes: (a) saltation: small particles move by jumping like leap-frog, Once lifted by wind it will drift downwind and return to hit the ground again and transfer energy and momentum to other soil aggregates (soil particles). (b) Creeping: large dust particles cannot be lifted into the air, but will just move and slide on the ground. (c) Suspension: if the upward draft is strong enough to compensate the gravitational force of the dust particles, dust will remain airborne and be transported by the wind over longer distances until its gravitational force overcome the uplifting force. It is believed that saltation is the main mechanism for surface dust emission (Shao et al., 1993; Marticorena and Bergametti, 1995).

Following Marticorena and Bergametti (1995) and Alfaro and Gomes (2001), a complex dust emission scheme has been implemented in RegCM3 (Zakey et al., 2006). This emission scheme is based on parameterization of soil aggregate saltation and sandblasting processes. According to this scheme, a critical parameter for the dust saltation process is the threshold friction velocity u_t^*, which is a function of particle size D_p (Eq. 1), such that, u_{ts}^* represents an ideal minimum threshold friction velocity, f_{eff} is a correction factor accounting for the effect of surface roughness and f_w is a factor that accounts for the effect of soil moisture content on the threshold friction velocity. The particle size is determined by the land surface soil texture. Calculating the threshold friction velocity is required to calculate the horizontal dust flux (dH_F) (Eq. 2), such that, E is the ratio of erodible to total surface, dS_{rel} is the relative surface of soil aggregate of diameter D_p to the total aggregate surface and $R(D_p)$ is the ratio of the threshold

ACPD
15, 1523–1571, 2015

friction velocity defined in (Eq. 1) to the friction velocity u^* calculated within each grid cell from the model prognostic surface wind and the surface roughness. Finally, the vertical dust emission flux dF_{kin} is assumed to be directly proportional to the horizontal flux dH_F (Eq. 3), such that, β is an empirical factor and its value is 16 300 cm s^{-2} (Zakey et al., 2006).

$$u_t^*\left(D_p\right) = u_{ts}^*\left(D_p\right) f_{eff} f_w \quad (1)$$

$$dH_F\left(D_p\right) = E\frac{\rho_a}{g}u^{*3}\left(1+R\left(D_p\right)\right)\left(1-R^2\left(D_p\right)\right)dS_{rel}\left(D_p\right) \quad (2)$$

$$dF_{kin}\left(R_p\right) = \beta dH_F\left(D_p\right) \quad (3)$$

Where, g is the gravity acceleration constant and ρ_a is air density. RegCM3 (a previous version) has been used frequently to simulate atmospheric dust and its radiative impact. Most of these simulations have been performed for areas in the Sahara (Zakey et al., 2006; Konarè et al., 2008; Solmon et al., 2008, 2012; Napat et al., 2012; Steiner et al., 2014), apart from one over East Asia (Zhang et al., 2009). Over the Middle East and Arabian Peninsula there have been a few studies such as (Marcella and Eltahir, 2010, 2011, 2012; Nazrul Islam and Almazroui, 2012).

2.2.3 Experimental design

The model simulations are conducted for 14 years (1999–2012), but the analysis is done for the 2000–2012 time period with the first year used for model spin-up. The European Centre for Medium Range Weather Forecasts Reanalysis project (ERA-Interim) reanalysis data (https://apps.ecmwf.int/datasets/data/interim_full_daily) has been used to provide the model with 6 h meteorological boundary conditions (Dee et al., 2011). Monthly climatology of dust aerosol is provided by the Model for Ozone and Related chemical Tracer (MOZART) model at 2.8° × 2.8° (T42) resolution (Emmons et al., 2010).

Figure 1 shows the model domain at 50 km grid resolution. The model vertical resolution is 18 sigma levels. The model physics is configured as follows; the boundary layer

ACPD
15, 1523–1571, 2015

scheme is UW-PBL, this is a 1.5 order local, down-gradient diffusion parameterization in which the velocity scale is based on the turbulent kinetic energy (TKE). The TKE in turn is calculated prognostically from the balance of buoyant production/destruction, shear production, dissipation vertical transport, and horizontal diffusion and advection (Giorgi et al., 2012; O'Brien et al., 2012).

The Bio-sphere-Atmosphere Transfer scheme (BATS) (Dickinson et al., 1993) is used to parameterize the land-surface atmosphere interaction. The full scheme includes a 1-layer vegetation module, a 1-layer snow module, a force restore model for soil temperature, a 3-layer soil scheme and a simple surface runoff parameterization. This scheme is simpler than the other CLM3.5 schemes in the model, which have many physical parameterizations of soil processes (Tawfik and Steiner, 2011). It does not require time for the soil to equilibrate with the atmosphere (Giorgi et al., 2012). The convection scheme provided by Grell (Grell, 1993) is used along with the Community Climate Model version 3 (CCM3) radiation scheme (Kiehl et al., 1996).

Figure 1a and b shows the BATS land texture and topography of the region. BATS land texture constitute of 17 categories (see Table 2 in Zakey et al., 2006). The first 16 categories represent the soil texture based on the classical sand-silt-clay percentage approach (Hillel, 2003). The stars indicate the location of the AERONET stations that will be used for model validation. The area around the AERONET stations will be used to calculate the area average of the modeled AOD for comparison against observations. S1 represents the Mesopotamian source region that includes Iraq and Arabian Peninsula, S2 represents the Red Sea source region that includes Al nofod desert, S3 represents the El Rob El khali desert, S4 represents the Somalia desert source region and S5 represents the southwest Asia source region that includes dry beds in the Afghanistan-Pakistan-Iran border.

ACPD
15, 1523–1571, 2015

3 AOD climatology

3.1 The annual cycle

Figure 2 shows the comparison between modeled AOD and observed MISR's AOD, for seasonal average.

The AOD is quite variable in space and time, yet shows a clear seasonal cycle. In September–December, the model and MISR have the lowest AOD (0.1–0.3). The AOD maximum (0.3) extends from northern Iraq to the southern part of the Arabian Peninsula up to the Arabian Sea. This maximum is in the vicinity of the Arabian Gulf and Najd plateau. The model and MISR show higher AOD over the Red Sea near the Bab-el-Mandab strait and parallel to the Yemen mountain ranges compared to the inland neighborhood. MISR's AOD is higher than the modeled AOD over the Arabian Sea due to the contribution of sea-salt aerosols.

In January–April, there is quite strong dust activity over the region of interest. The AOD increases over all source regions (S1, S2, S3, S4 and S5; for locations see Fig. 1a with variable magnitudes. The AOD ranges from 0.3 to 0.5, the band of the highest AOD lies between the Arabian Gulf and Najd plateau. The band has a tongue shape extended inside Iraq (S1) and has a flattened base near the El Rob El khali desert (S3). The Somalia (S4) and Iran-Pakistan-Afghanistan (S5) dust sources do not contribute too much to the AOD over the entire region.

The model's AOD spatial distribution is quite similar to MISR, yet overestimates AOD around the S1, S2 and S5 dust sources in January–April, In April, the model and MISR results become close to each other. During February–April, the model shows systematic decrease of AOD off the southern coast of the Arabian Peninsula; however, MISR shows higher AOD over the Indian Ocean/Arabian Sea, which may be attributed to sea salt aerosol.

In the May–August months the AOD reaches its maximum (0.5–0.9). In May the maximum AOD band is between the Arabian Gulf and Najd Plateau. This band migrates

ACPD
15, 1523–1571, 2015

southward south in July–August. The AOD over the Red Sea and the Gulf of Aden increases steadily and reaches its maximum in July.

The model shows a comparable spatial distribution, yet overestimates AOD values. The modeled AOD maximum is centered over El Rob El khali desert (S3) in the south-eastern Arabian Peninsula. The AOD spatial distribution is controlled mainly by the topography of the region. The eastern Arabian Gulf high land that extends from the Anatolia plateau in Turkey to southern Iran parallel to the Arabian Gulf (Fig. 1b) and the Najed Plateau in the central Arabian Peninsula (Fig. 1b) act as a funnel that controls the wind flow system in that complex region. The MISR AOD shows such a banana-like shape for the spatial distribution of maximum AOD; model's AOD shows this shape to a certain extent. In June, July and August, the model underestimates the AOD in the northern part of the Peninsula especially in Iraq, Jordan and Kuwait. However, the model overestimates AOD in the southeastern part of the Arabian Peninsula over Yemen, Oman and UAE.

The analysis of the annual cycle of the zonally averaged AOD reveals interesting features of the temporal AOD development across the domain. Figure 3a represents the zonally averaged AOD (36–50° E) and the area of interest spans from 10–30° N. The model shows a first maximum in March and April centered at 25° N, the model's AOD decreases in April and start to increase again in May. The second maximum is in mid-summer (July) and centered between 10 and 20° N. This second maximum reveals two peaks: one represents the southern Arabian Peninsula dust sources (15–20° N) and the other one the Somalia dust sources (10–15° N); the minimum in between is the Bab-Elmandab strait and Gulf of Aden.

The MISR annual cycle of the zonally averaged AOD shows a bit different distribution (Fig. 3b). The first maximum is in between April and May and is centered at 28° N. The second maximum is in July and is centered between 10 and 20° N. It has two peaks, however they are not clear as MISR, one represents the Arabian Peninsula dust sources and the other represents the Somalia dust sources. The analysis of the large-scale circulation provides a plausible explanation of such a bi-modal behavior.

ACPD
15, 1523–1571, 2015

3.2 Comparisons with AERONET and satellite observations

The modeled AOD has been compared with different instruments, namely, MISR, MODIS (Deep-blue), OMI and AERONET. The three AERONET stations (details shown in Supplement Table S1) show differences in the AOD's seasonal cycle, magnitude and monthly variability. The modeled AOD is from dust aerosol alone, however the measured AOD is a result of all kind of aerosol present in the region (e.g., black carbon, sulfate and sea-salt). This should be considered as a source of discrepancy. Nevertheless, in spring and summer dust aerosol is the major aerosol component over the Arabian Peninsula (Kim et al., 2011).

In the following discussion the dust season for a given site is defined as those months that have at least 20 % higher AOD values compared to the annual mean AOD at that site. The first row in Table 1 shows the annual mean of the medians for each dataset for each station, the following rows represent the calculated monthly deviation from this annual median. The deviation from the annual mean is calculated by the following equation

$$\text{deviation} = 100 \times \frac{\tau_{\text{month}} - \tau_{\text{annual}}}{\tau_{\text{annual}}} \quad (4)$$

where τ_{month} is the AOD monthly average and τ_{annual} is the AOD annual mean.

The modeled AOD showed different behavior with respect to each observational dataset as well as station's location. Table 2 shows the modeled monthly median for each site (shown in the first column for each site) and the corresponding relative error ($\text{Error}_{\text{rel}}$) calculated using the following equation.

$$\text{Error}_{\text{rel}} = 100 \times \frac{\tau_{\text{m}} - \tau_{\text{o}}}{\tau_{\text{m}}} \quad (5)$$

with τ_{m} being the modeled AOD and τ_{o} being the observed AOD. The negative (positive) relative error means how much the model is underestimated (overestimated) with respect to a given observation.

ACPD
15, 1523–1571, 2015

3.2.1 Kuwait University, Kuwait

The Kuwait University site is near major dust sources (S1 and S2 in Fig. 1a) and would be representative to the northern Arabian Peninsula dust aerosol climatology. Figure 4 shows a 5 year statistics of AOD for AERONET station, a 7 years statistics of AOD for the satellite observations and a 13 year statistics of AOD for RegCM4.

Table 1 shows that the AERONET annual averaged median is ~ 0.4. Therefore the dust season months, which exceed 20 % of the annual averaged median are April–July (Table 1). May shows the maximum AOD, which is 50 % higher than the annual average. The May–July months show a maximum variability (the difference between 25 percentile and 75 percentile is the greatest). December and January show a minimum AOD of 0.2 (Fig. 4).

The observational dataset shows some disagreement about the length and intensity of the dust season according to the proposed criterion. AERONET and MISR show four months as dust season, while MODIS and OMI only show three month as dust season. In addition AERONET and MISR AOD values are often higher than the MODIS and OMI AOD values.

3.2.2 Solar-Village, Saudi Arabia

The Solar-Village site would be a representative of central Arabian Peninsula dust aerosol climatology. The altitude of this site (764 m a.s.l) and its location in the vicinity of complex terrain may contribute to the apparent differences in AOD climatology with regard to the other sites. Figure 5 shows a 13 year statistics of AERONET AOD, a 7 year statistics of AOD for the satellite observations and a 13 year statistics of RegCM4 AOD.

The satellite group shows maximum AOD in March–June, except for OMI, whose maximum AOD occur in February–August. In addition, OMI has higher AOD values than the other satellite platforms. AERONET shows maximum median in April–August months and underestimates the AOD (Fig. 5).

ACPD
15, 1523–1571, 2015

The AERONET AOD statistics show that the AOD annual average median is 0.27 (Table 1). Since dust concentration decreases with height, therefore The AERONET AOD of Solar-Village is much less than the Kuwait University site and this may be due to the high altitude of Solar-Village and its far distance to major dust sources. Nevertheless, this station could capture a severe dust episode as reported by Alharbi et al. (2013) and Kalenderski et al. (2013).

The dust season in this region spans five months (April–August) according to the AERONET data; however, MODIS, MISR and OMI show April–June months as the dust season (Table 3). MODIS, MISR and OMI show higher AOD than AERONET for Solar-Village at the time of the dust season (Fig. 5).

Solar-Village shows a different climatology in terms of the dust season onset and its intensity. The model shows a larger temporal extension of the dust season and an early onset; it starts in March and lasts until August.

3.2.3 Mezaira, United Arab Emirate (UAE)

The Mezaira site is near the El rob El khali desert, which is a major dust source in the Arabian Peninsula (S3 in Fig. 1a). The site is representative for southern Arabian Peninsula dust aerosol climatology.

Figure 6 shows a 7 year statistics of AERONET AOD, 7 year statistics of AOD for the satellite observations and a13 year statistics of AOD for RegCM4.

The annual average median is ~ 0.4 (Table 1). The extension of the dust season varies among the datasets, AERONET shows 5 months dust season (April–August), MISR and OMI show 4 months dust season (May–August), MODIS shows 3 months dust season (June–August) and finally RegCM4 shows a 2 months dust season (July–August). They all agree about the end of the dust season in August but they disagree on the dust season onset (Table 1).

Different regions in the Arabian Peninsula have different dust aerosol climatology. The main feature of this climatology is the forward time shift of the dust season towards the south of the Arabian Peninsula. This feature is evident in Fig. 3. The quantitative

ACPD
15, 1523–1571, 2015

analysis in Table 1 also reflects this phenomenon in all datasets. Table 1 shows how the dust season is shifted towards summer months along the traverse from the northern (Kuwait site) to the southern part of the Arabian Peninsula (UAE site). This feature will be explained by the analysis of the atmospheric dynamics in the following section.

The validation of the modeled AOD against the observations shows how the model behaves differently from region to region and could shed some light on the sources of uncertainty of the model. Table 2 (first column for each site) lists the modeled AOD monthly medians for the three sites and it is used to calculate the relative error with respect to each observational datasets according to Eq. (5).

RegCM4 underestimates AOD over the northern part of the Arabian Peninsula with respect to all observational datasets (Table 2). For the dust season months (April–July) the model relative error ranges between 29 and 68 %. This model feature is also noticed in Marcella and Eltahir (2010). Toward the central Arabian Peninsula, the model performance becomes better, and the relative error is between 7 and 60 %. The model underestimates in the late spring season, but tends to overestimate in the summer season (Table 2). Toward the southern Arabian Peninsula, the model error ranges reduced compared to the other stations, for instance, the model errors in June are 1 and 5 % with respect to AERONET and MODIS respectively. On the other hand, the model shows significant over estimation in August, which is as high as 90 and 75 % with respect to AERONET and MODIS, respectively (Table 2).

4 Spatial and temporal dust evolution

The large-scale circulation ultimately controls the seasonal evolution of atmospheric mineral dust. However, the topography and dust source distributions provide the surface boundary conditions that determine the intensity of surface dust emission and eventually the intensity of the dust storm.

The synoptic features promoting dust storms are different in spring than in summer. In springtime most dust storms are a result of frontal systems that overpass potential

ACPD
15, 1523–1571, 2015

dust sources in northern Arabia. There are two types of frontal type dust, pre-frontal type and post-frontal type (Wilkerson, 1991). The frontal system is associated with instability of the air column, which results in dust uplifting. The summertime dust storm is a result of strong north to northwest wind associated with the Indian monsoon depression.

4.1 Spring time (cold season)

4.1.1 Large-scale circulation

In winter and early spring (January–April) the Arabian Peninsula is affected by an extension of Siberian High pressure and the Red Sea trough in northern part and southern part of the Arabian Peninsula respectively. The anti-cyclonic wind field is dominated over the Arabian Peninsula. Figure 7a and b shows the climatology of the mean sea level pressure (MSLP), while Fig. 7d and e shows the climatology of temperature and wind field at 850 hPa geopotential surface. While the extension of Siberian high pressure with cold air mass affects the northern part of the Arabian Peninsula (Fig. 7a and b), the southerly winds which are associated with the Red Sea trough over the southern Arabian Peninsula advect warm air toward north (Fig. 7d and e), which leads to instabilities in the atmosphere.

The position and strength of the Sub-Tropical Jet (STJ) at 200 hPa determine the atmospheric stability at the surface. Figure 7g and h shows the climatology of the STJ. In winter the STJ core is located over the Arabian Peninsula. The spring STJ core is weaker than the winter STJ. It migrates toward north in April–May and displays a strong meridional component (Fig. 7g and h). Alhabri et al. (2013) described the role of the STJ in the onset and development of dust storms. Briefly, the STJ generates regions of upward motion and downward motion (i.e. secondary circulation). The north side of the STJ core is a divergence zone that is associated with upward motion, while the south of the STJ core is a conversion zone that is associated with downward motion. Figure 8 shows the zonally averaged vertical velocity (Omega in hPa s^{-1} where

ACPD
15, 1523–1571, 2015

(−) values designate upward motion and (+) values designate downward motion). In December–April the STJ core is located south of 30° N (Fig. 7g and h), and Fig. 8 shows the secondary circulation region of upward motion and downward motion from surface (1000 hPa) to the upper air (100 hPa) south of 30° N. In late winter (February) and spring time (March–April) the upward motion progressively strengthens from 20° N to 30° N and from surface to upper air levels.

In most part of the Arabian Peninsula, the prevailing wind directions are southerlies and southwesterlies. The observations over the northern and southern parts of the Arabian Peninsula show that during the dust season, the prevailing wind directions are southerlies and southwesterlies (Mashat et al., 2008). Figure 9 shows the climatology of the zonally averaged wind's meridional component. The southerly meridional component shows the ascending motion and the sliding of warm air over the cold air from the north.

Figure 10 shows the climatology of the zonally averaged vertical profile of fine dust concentration. The maximum concentration is located between 15 and 30° N. The dust concentrations progressively increase towards north from December to February and start to retreat in April. In winter and spring, dust layers do not extend to high levels in the atmosphere, actually they are confined to levels below 800 hPa.

4.1.2 Land surface response

The friction velocity is the sole dynamical variable in the dust parameterization (the other variables are land surface characteristics). The land surface response of the large scale circulation is reflected by the friction velocity. Also, according to Eqs. (2) and (3), the dust emission is proportional to the friction velocity. In Supplement Fig. S1 the friction velocity over land surfaces is shown and in the following discussion, we will focus in particular on the dust source regions (Fig. 1a).

In the late winter and early spring months (January–March) the friction velocity is high in the western and central part of the Arabian Peninsula (Fig. S1). Correspondingly, dust emissions are also higher in the western and central Arabian Peninsula com-

ACPD
15, 1523–1571, 2015

pared to the surrounding areas (Fig. 11). Over the source region S4 (Al Roub AL khali desert) dust emission is clearly accompanied with high friction velocity. In the northern part of the Arabian Peninsula the climatology of the friction velocity does not reflect the abovementioned relation between friction velocity and surface dust emission. Although, this region is affected by a high pressure system which causes a weak surface wind field, most of the emitted dust in this region is due to a fast migrating cyclone over the Syria–Iraq area associated with high surface wind (Mashat et al., 2008; Abdi Vishkaee et al., 2012; Alharbi et al., 2013) that has been filtered out in the averaging procedure.

The corresponding atmospheric surface dust concentration for dust less than 10 µm is shown in Fig. S2. In the months from December to April the surface dust concentration over the Arabian Peninsula reaches up to 120 $\mu g\,m^{-3}$ in the central region, which is in agreement with results for the same region performed in a global modeling study by Ginoux et al. (2004).

4.2 Summer time (warm season)

4.2.1 Large-scale circulation

Starting mid-spring (i.e. April) the surface high pressure retreats and the Indian Monsoon depression starts to progress towards the Arabian Peninsula. In summer (June–August) the Arabian Peninsula is largely impacted by the Indian Monsoon depression and it further intensifies during summer months (Fig. 7c). The prevailing winds in this season are northerlies and northwesterlies ("Shamal") over the most of the Arabian peninsula (Mashat et al., 2008), while the southern part is affected by strong southerly winds associated with the Low-Level Jet (i.e. Somalia Jet) that is triggered by the Indian Monsoon (Fig. 7f). In late spring and summer (i.e. April–August), the STJ migrates toward north and a high pressure is develops over the Arabian Peninsula (Fig. 7i).

The summer meridional components in Fig. 9 become northerly, which is an indication of the Indian Monsoon cyclonic circulation. In addition, Fig. 8 shows that the ascending motion in the southern part of the Arabain Peninsula (15–25° N) is higher

ACPD
15, 1523–1571, 2015

than during the winter-spring time. The descending motion over the ocean is evident in the summer season at latitudes from 10 to 15° N. According to Fig. 10 the ascending motion in southern Arabia in upper air results in uplifting of dust to higher atmospheric levels up to the 500 hPa level. After the retreat of the Indian Monsoon, the ascending motion weakens significantly and the meridional velocity reverses its sign to be southerly again.

4.2.2 Land surface response

During the summer season, starting June, the friction velocity (Fig. S1) gets higher in the eastern and southern part of the Arabian Peninsula, and over Somalia (dust sources S3 and S4 in Fig. 1a). As a consequence high surface dust emission fluxes (Fig. 11) occur over the eastern and the southern Arabian Peninsula (e.g. in Oman) and over Somalia. Those source regions contribute significantly to the resultant AOD in summer. The surface dust concentration in summer reaches maximum values between 100–180 $\mu g\,m^{-3}$ (Fig. S2).

5 Dust radiative impact

The ultimate aim of studying the climatology of aerosol in any climate chemistry model like RegCM4 is to estimate the radiative feedback of aerosol on climate (Stanelle et al., 2010), namely, the radiative forcing of the aerosol. With regard to some Global Climate Model (GCM) simulations, the principal radiative effect of mineral dust is heating the atmosphere in the source region. This results in inhibiting convection and reduction in precipitation (Tegan and Lacis, 1996). The analysis of radiative forcing and its dependence on particle size shows that regardless of the particle size dust particles exert negative radiative forcing (cooling effect) near the Earth's surface. However, such negative radiative forcing decreases with height according to the dust particle's radius. The radiative forcing becomes positive (heating effects) for larger particle at higher levels

ACPD
15, 1523–1571, 2015

(Tegan and Lacis, 1996). In this study we only estimate the direct radiative forcing of dust aerosol, since there is no indirect effect parameterization in RegCM4.

In the following sections we will compare the model's estimation of the Top of Atmosphere Radiative forcing (TOARF) and the Bottom of the Atmosphere Radiative Forcing (BOARF) with the AERONET's BOARF and TOARF inversion products (Dubovik and King, 2000). The AERONET BOARF and TOARF calculation based on the "Almucantar" basic sky measurement at optical air mass equal to 2–4 (i.e. the zenith angle between 50° and 80°) provides highest accuracy for the aerosol properties retrieval algorithm (Holben et al., 1998; García et al., 2012). For this condition we do not compare observations with daily average or noon-time modeled radiative forcing, but only select the afternoon model output (i.e. the 15:00 and 18:00 UTC output). The AERONET's BOARF and TOARF is retrieved for the shortwave range between (0.44–1.02 µm) and we compare this data with model's surface shortwave range between radiative forcing and TOA shortwave radiative forcing.

5.1 BOARF

Figure 12 shows the comparison between the AERONET stations and RegCM4 for (BOARF). While RegCM4 captures the peak of seasonal cycle of BOARF (April–August), it clearly underestimates BOARF for all months. The Kuwait AERONET station shows the largest BOARF median (up to $-90\,W\,m^{-2}$ in June) compared to Solar-Village (June median: $-61\,W\,m^{-2}$) and UAE-Mazeira (June median up to $-62\,W\,m^{-2}$). On the other hand, the model's area averaged AOD values around the AERONET station locations shows lower values in June; the median for Kuwait is $\sim -19\,W\,m^{-2}$, while for both, Solar-Village and UAE-Mezaira the median is $\sim -20\,W\,m^{-2}$. These experiment results are close to other modeling results (e.g., Kalenderski et al., 2013 estimates BOARF around $-15.0\,W\,m^{-2}$ for a winter dust storm over the Arabian Peninsula using WRF model). But it seems that RegCM4 underestimates BOARF in other regions like North Africa as shown by Napat et al. (2012), who calculate around $-15.0\,W\,m^{-2}$ for BOARF in May. The comparison between the modeled and observed annual BOARF

ACPD
15, 1523–1571, 2015

(expressed as the average of monthly medians) as displayed in Table 3 shows that the Kuwait University site has the largest observed BOARF ($-65\,W\,m^{-2}$), while the modeled BOARF does not show big differences among the three regions. On the average, RegCM4 underestimates BOARF by a factor of 4 (Table 3).

The seasonal behavior of the model shows a negative radiative forcing (cooling effects) over the whole domain with maximum negative radiative forcing over the Arabian Peninsula and Somalia compared to other regions with relatively high dust concentration like Pakistan or the Caspian sea regions (Fig. S3). This is, because dust in those regions does not extend to upper air like it is the case over the Arabian Peninsula (Fig. 10).

5.2 TOARF

Figure 13 shows the comparison of TOARF between the AERONET stations and RegCM4. The effect of dust in this case is controversial. The TOARF is generally less negative than the BOARF and even may become positive. This depends on the prescribed optical properties like the single scattering albedo and the complex refractive index in the model and also the AERONET retrieval algorithm. This positivity is indicative on how the mineral dust aerosol heats the atmosphere. García et al. (2012) show that the AERONET retrieved TOARF is exclusively negative over the Arabian Peninsula region. However, our analysis for the AERONET data yields positive values only for extreme values not within the 75 percentile (Fig. 13). The Kuwait University site has the largest negative values of TOARF (up to $-25\,W\,m^{-2}$). Solar-Village has $-10\,W\,m^{-2}$ and UAE-Meziara has $-13\,W\,m^{-2}$. The model underestimates TOARF: up to $-5\,W\,m^{-2}$ over the Kuwait site, $-4\,W\,m^{-2}$ over Solar-Village and $-7\,W\,m^{-2}$ over UAE-Meziara. The comparison between modeled and the observed annual TOARF (expressed as the average of the monthly median) indicates that again the Kuwait site exhibits the largest observed TOARF ($-17\,W\,m^{-2}$), while the modeled TOARF does not show big differences among the three regions (see Table 3). On the average, RegCM4 underestimates the TOARF by a factor of 3 (Table 3).

ACPD
15, 1523–1571, 2015

Figure S4 displays the seasonal evolution of TOARF. There are pronounced negative values over the sea surface, but, over land surface the TOARF signal is close to zero or may even become positive over the center of the Arabian Peninsula especially in July. This feature is related to the underlying land surface albedo, where the Arabian Peninsula has a higher surface albedo that contributes to TOARF.

6 Summary and conclusions

The Regional Climate Model version 4 (RegCM4) has been used to simulate the occurrence and distribution of atmospheric mineral dust aerosol over the Arabian Peninsula. Thirteen years of high resolution simulation and a comparison with a suite of observational datasets were utilized to understand the climatology of atmospheric dust occurrence. Observational data included Kuwait University, Solar-Village and UAE-Mezaira AERONET stations, having the longest AOD record, and.satellite AOD retrievals from MISR, OMI and MODIS (Deepblue) from 2006 to 2012.

While the modeled AOD shows that the dust season extends from March to August with two pronounced maxima, one over the northern Arabian Peninsula in March (AOD ≈ 0.4) and one over the southern Arabian Peninsula in July (AOD ≈ 0.7), the observations indicate a dust season, which extends from April to August with two pronounced maxima, one over the northern Arabian Peninsula in April (AOD ≈ 0.5) and one over the southern Arabian Peninsula in July (AOD ≈ 0.5). The zonally averaged annual cycle AOD analysis shows two AOD peaks, one in springtime (March–May) and one in summertime (June–August). While the model and the observations agree in the timing of the summertime peak, there is some disagreement in the springtime peak where the model reveals a springtime peak about, one month earlier (February–March). This bi-modal oscillation of dust occurrence is caused by the large scale circulation and the land surface response.

In spring the Arabian Peninsula is under the influence of the Siberian high from the north and north-east and the extension of the Red Sea trough from the south and

ACPD
15, 1523–1571, 2015

south-west. The frontal area between the cold air in the north and warm air in the south promotes a strong southerly wind with enhanced upward motion, which results in dust uplifting in the northern and western part of the Arabian Peninsula. This is favored by increased surface friction in these areas at the same time.

In summer the atmospheric circulation entirely changes. The Arabian Peninsula is affected by the extension of Indian Monsoon Depression that causes the Shamal, a strong northwesterly wind aligned along the Arabian Gulf. The Shamal is strong enough to push and concentrate dust over the southern part of the Arabian Peninsula. At the same time the Somalia Low-Level Jet strongly enhances the dust uplifting from dust sources in Somalia. The Somalia dust contributes significantly to the overall dust burden over the region, especially over the Red and Arabian Sea.

The Top of Atmosphere Radiative Forcing (TOARF) and the Bottom of Atmospheric Raditive Forcing (BOARF) data retrieved from AERONET were used to analyze the atmospheric dust radiative forcing to obtain a better understanding of potential climate feedback mechanisms in the region. While the model captures the annual cycle of TOARF and BOARF, it underestimates both by a factor of 3 and 4, respectively. These biases contribute to the large uncertainty of modeled surface temperature over the Arabian Peninsula noticed earlier by Steiner et al. (2014).

Overall, the seasonal behavior of BOARF shows a negative radiative forcing with a maximum in the summer (cooling effects) over the whole domain and with maximum negative radiative forcing over the Arabian Peninsula and Somalia compared to other regions with relatively high dust concentration like Pakistan or the Caspian Sea region. Our study indicates that this is due to the fact that dust in those regions does not extend to upper air like it is the case over the Arabian Peninsula.

The model's TOARF is less negative and may even display some positivity in the central region of the Arabian Peninsula. The analysis of the observed and modeled TOARF shows that, it is essential to consider the surface albedo of the region. With the high surface albedo of the central Arabian Peninsula, mineral dust aerosols tend to warm the atmosphere in summer (June–August).

ACPD
15, 1523–1571, 2015

The Supplement related to this article is available online at doi:10.5194/acpd-15-1523-2015-supplement.

Acknowledgements. We gratefully acknowledge the data provided by the AERONET network and we wish to express our appreciation to the operators of stations for maintaining these important measurements.

References

Abdou, W. A., Diner, D. J., Martonchik, J. V., Bruegge, C. J., Kahn, R. A., Gaitley, B. J., Crean, K. A., Remer, L. A., and Holben, B.: Comparison of coincident multiangle imaging spectroradiometer and moderate resolution imaging spectroradimeter aerosol optical depths over land and ocean scenes containing aerosol robotic network sites, J. Geophys. Res., 110, D10S07, doi:10.1029/2004JD004693, 2005.

Abdi Vishkaee, F., Flamant, C., Cuesta, J., Oolman, L., Flamant, P., Khalesifard, H.: Dust transport over Iraq and northwest Iran associated with winter shamal: a case study, J. Geophys. Res., 117, D03201, doi:10.1029/2011JD016339, 2012.

Alfaro, S. C., and Gomes, L.: Modeling mineral aerosol production by wind erosion: emission intensities and aerosol size distribution in source areas, J. Geophys. Res., 106, 18075–18084, 2001.

Alharbi, B. H.: Airborne dust in Saudi Arabia: source areas, entrainment, simulation and composition, PhD dessertation, Monash university, Melbourne, Australia, 313 pp., 2009.

Alharbi, B. H., Maghrabi, A., and Tapper, N.: The march 2009 dust event in Saudi Arabia: precursor and supportive environment, B. Am. Meteorol. Soc., 94, 515–528, 2013.

Dee, D. P., Uppala, S. M., Simmons, A. J., Berrisford, P., Poli, P., Kobayashi, S., Andrae, U., Balmaseda, M. A., Balsamo, G., Bauer, P., Bechtold, P., Beljaars, A. C. M., Van de Berg, L., Bidlot, J., Bormann, N., Delsol, C., Dragani, R., Fuentes, M., Geer, A. J., Haimberger, L., Healy, S. B., Hersbach, H., Hólm, E. V., Isaksen, L., Kållberg, P., Köhler, M., Matricardi, M., McNally, A. P., Monge-Sanz, B. M., Morcrette, J.-J., Park, B.-K., Peubey, C., de Rosany, P., Tavolato, C., Thépaut, J.-N., and Vitart, F.: The ERA-interim reanalysis: configuration and performance of the data assimilation system, Q. J. Roy. Meteor. Soc., 137, 553–597, 2011.

ACPD
15, 1523–1571, 2015

Dickinson, R. E., Henderson-Sellers, A., and Kennedy, P. J.: Biosphere–atmosphere transfer scheme version 1e as coupled to the NCAR community climate model, Tech. Rep., National Center for Atmos. Res., Boulder, Colorado, USA, 1–80, 1993.

Diner, D. J., Beckert, J. C., Reilly, T. H., Bruigge, C. J., Conel, J. E., Kahn, R. A., Martonchik, J. V., Acherman, T. P., Davies, R., Gerstl, S. A. W., Gordon, H. R., Muller, J., Myneni, R. B., Sellers, P. J., Pinty, B., and Verstraete, M. M.: Multi-angle imaging spectroradiometer (misr) instrument description and experiment overview, IEEE T. Geosci. Remote, 36, 1072–1087, 1998.

Dubovik, O. and King, M. D.: A flexible inversion algorithm for retrieval of aerosol optical properties from Sun and sky radiance measurements, J. Geophys. Res., 105, 20673–20696, 2000.

Eck, T. F., Holben, B. N., Reid, J. S., Sinyuk, A., Dubovik, O., Smirnov, A., Giles, D., O'Neill, N. T. N., Tsay, S.-C., Ji, Q., Mandoos, A. A., Khan, M. R., Reid, E. A., Schafer, J. S., Sorokine, M., Newcomb, W., and Slusker, I.: Spatial and temporal variability of column-integrated aerosol optical properties in the southern Arabian Gulf and United Arab Emirates in summer, J. Geophys. Res, 113, D01204, doi:10.1029/2007JD008944, 2008.

Emmons, L. K., Walters, S., Hess, P. G., Lamarque, J.-F, Pfister, G. G., Fillmore, D., Granier, C., Guenther, A., Kinnison, D., Laepple, T., Orlando, J., Tie, X., Tyndall, G., Wiedinmyer, C., Baughcum, S. L., and Kloster, S.: Description and evaluation of the model for ozone and related chemical tracers, version 4 (MOZART-4), Geosci. Model Dev., 3, 43–67, 2010.

García, O. E., Díaz, J. P., Expósito, F. J., Díaz, A. M., Dubovik, O., Derimian, Y., Dubuisson, P., and Roger, J.-C.: Shortwave radiative forcing and efficiency of key aerosol types using AERONET data, Atmos. Chem. Phys., 12, 5129–5145, doi:10.5194/acp-12-5129-2012, 2012.

Giannadaki, D., Pozzer, A., and Lelieveld, J.: Modeled global effects of airborne desert on air quality and premature mortality, Atmos. Chem. Phys. 14, 957–968, doi:10.5194/acp-14-957-2014, 2014.

Giorgi, F. and Bates, G. T.: The climatological skill of a regional model over complex terrain, Mon. Weather Rev., 117, 2325–2347, 1989.

Giorgi, F., Bates, G. T., and Nieman, S. J.: The multi-year surface climatology of a regional atmospheric model over the western United States, J. Climate, 6, 75–95, 1993a.

ACPD
15, 1523–1571, 2015

Giorgi, F., Marinucci, M. R., and Bates, G. T.: Development of a second generation regional climate model (regcm2) i: boundary layer and radiative transfer processes, Mon. Weather Rev., 121, 2794–2813, 1993b.

Giorgi, F., Coppola, E., Solmon, F., Mariotti, L., Sylla, M. B., Bi, X., Elguindi, N., Diro, G. T., Nair, V., Giuliani, G., Turuncoglu, U. U., Cozzini, S., Guttler, I., O'Brien, T. A., Tawfik, A. B., Shalaby, A., Zakey, A. S., Steiner, A. L., Stordal, F., Sloan, L. C., and Brankovic, C.: RegCM4: model description and preliminary tests over multiple CORDEX domains, Clim. Res., 52, 7–29, doi:10.3354/cr01018, 2012.

Ginoux, P., Prospero, J. M., Torres, O., and Chin, M.: Long term simulation of global dust distribution with the GOCART model: correlation with north Atlantic oscillation, Environ. Modell. Softw., 19, 113–128, 2004.

Gobbi, G. P., Barnaba, F., and Ammannato, L.: The vertical distribution of aerosols, Saharan dust and cirrus clouds in Rome (Italy) in the year 2001, Atmos. Chem. Phys., 4, 351–359, 2004, http://www.atmos-chem-phys.net/4/351/2004/.

Grell, G.: Prognostic evaluation of assumptions used by cumulus parameterization, Mon. Weather Rev., 121, 764–787, 1993.

Hillel, D.: Introduction to environmental soil physics, Academic Press, Massachusetts, USA, 494 pp., 2003.

Holben, B. N., Eck, T. F., Slutsker, I., Tanre, D., Buis, J. P., Setzer, A., Vermote, E., Reagan, J. A., Kaufman, Y. J., Nakajima, T., Lavenu, F., Jankowiak, I., and Smirnov, A.: AERONET A federated Instrument network and data archive for aerosol characterization, Remote Sens. Environ., 66, 1–16, 1998.

IPCC: Climate Change 2013: The Physical Basis. Contribution of Working Group I to the Fifth Assessment Report of the Intergovernmental Panel on Climate Change, edited by: Stocker, T. F., Qin, D., Plattner, G.-K., Tignor, M., Allen, S. K., Boschung, J., Nauels, A., Xia, Y., Bex, V., and Midgley P. M., Cambridge University Press, Cambridge, United Kingdom and New York, USA, 1535 pp., 2013.

Kalenderski, S., Stenchikov, G., and Zhao, C.: Modeling a typical winter-time dust event over the Arabian Peninsula and the Red Sea, Atmos. Chem. Phys., 13, 1999–2014, doi:10.5194/acp-13-1999-2013, 2013.

Kiehl, J. T., Hack, J. J., Bonan, G. B., Boville, B. A., Breigleb, B. P., Williamson, D., and Rasch, P.: Description of the NCAR community climate model (CCM3), Tech. Rep.

ACPD
15, 1523–1571, 2015

NCAR/TN-420+STR, National Center for Atmospheric Research, Boulder, Colorado, USA, 1–159, 1996.
Kim, D., Chin, M., Yu, H., Eck, T. F., Sinyuk, A., Smirnov, A., and Holben, B. N.: Dust optical properties over North Africa and Arabian Peninsula derived from the AERONET dataset, Atmos. Chem. Phys., 11, 10733–10741, doi:10.5194/acp-11-10733-2011, 2011.
Konarè, A., Zakey, A. S., Solmon, F., Giorgi, F., Rausher, S., Ibrah, S., and Bi, X.: A regional climate modeling study of the effect of desert dust on the west African monsoon, J. Geophys. Res., 113, D12206, doi:10.1029/2007JD009322, 2008.
Koren, I., Kaufman, Y. J., Washington, R., Todd, M. C., Rudich, Y., Martins, J. V., and Rosenfeld, D.: The bodélé depression: a single spot in the Sahara that provides most of the mineral dust to the Amazon forest, Environ. Res. Lett., 1, 014005, doi:10.1088/1748-9326/1/1/014005, 2006.
Levelt, P. F., Hilsenrath, E., Leppelmeier, G. W., van den Oord G. H. J., Bhartia, P. K., Tamminen, J., de Haan, J. F., and Veefkind, J. P.: Science objectives of the ozone monitoring instrument, IEEE T. Geosci. Remote, 44, 1199–1208, 2006.
Marcella, M. P. and Eltahir, E. A. B.: Effects of mineral aerosols on the summertime climate of southwest Asia: incorporating subgrid variability in a dust emission scheme, J. Geophys. Res., 115, D18203, doi:10.1029/2010JD014036, 2010.
Marcella, M. P. and Eltahir, E. A. B.: The role of lateral boundary conditions in simulations of mineral aerosols by a regional climate model of southwest asia, Clim. Dynam., 38, 109–120, doi:10.1007/s00382-010-0992-y, 2011.
Marcella, M. P. and Eltahir, E. A. B.: Modeling the summertime climate of southwest Asia: the role of land surface processes in shaping the climate of semiarid regions, J. climate, 25, 704–719, 2012.
Marchand, R., Ackerman, T., Smyth, M., and Rossow, W. B.: A review of cloud top height and optical depth histograms from MISR, ISCCP, and MODIS, J. Geophy. Res., 115, D16206, doi:10.1029/2009JD013422, 2010.
Marey, H. S., Gille, J. C., El-Askary, H. M., Shalaby, E. A., and El-Reay, M. E.: Aerosol climatology over Nile Delta based on MODIS, MISR and OMI satellite data, Atoms. Chem. Phys., 11, 10637–10648, doi:10.5194/acp-11-10637-2011, 2011.
Marticorena, B. and Bergametti, G.: Modeling the atmospheric dust cycle: 1. design of a soil-derived dust emission scheme, J. Geophys. Res., 100, 16415–16430, 1995.

ACPD
15, 1523–1571, 2015

Martonchik, J. V., Diner, D. J., Kahn, R., Acherman, T. P., Verstraete, M. M., Pinty, B., and Gordon, H. R.: Techniques for the retrieval of aerosol properties over land and ocean using multiangle imaging, IEEE T. Geosci. Remote, 36, 1212–1227, 1998.

Martonchik, J. V., Diner, D. J., Kahn, R., Gaitley, B., and Holben, B. N.: Comparison of MISR and AERONET aerosol optical depth over desert sites, Geophys. Res. Lett., 31, L16102, doi:10.1029/2004GL019807, 2004.

Mashat, A. S., Alamodi, A. O., and Ahmed, H. A. M.: Diagnostic and prognostic study for dust (sand) storms over Saudi Arabia, Tech. Rep. V18_AR-26–89, King Abdulaziz University, Faculty of Meteorology, Environment and Arid Land Agriculture, Saudi Arabia, 2008.

Napat, P., Solmon, F., Mallet, M., Kok, J. F., and Somot, S.: Dust emission size distribution impact on aerosol budget and radiative forcing over the Mediterranean region: a regional climate model approach, Atoms. Chem. Phys. 12, 10545–10567, doi:10.5194/acp-12-10545-2012, 2012.

Nazrul Islam, M. and Almazroui, M.: Direct effect and feedback of desert dust on the climate of the Arabian Peninsula during the wet season: a regional climate model study, Clim. Dynam., 39, 2239–2250, doi:10.1007/s00382-012-1293-4, 2012.

O'Brien, T. A., Chuang, P. Y., Sloan, L. C., Faloona, I. C., and Rossiter, D. L.: Coupling a new turbulence parameterization to RegCM adds realistic stratocumulus clouds, Geosci. Model Dev., 5, 989–1008, doi:10.5194/gmd-5-989-2012, 2012.

Pal, J. S., Giorgi, F., Bi, X., Elguindi, N., Solmon, F., Gao, X., Rauscher, S. A., Francisco, R., Zakey, A., Winter, J., Ashfaq, M., Syed, F. S., Bell, J., Diffenbaugh, N., Karmacharya, J., Martinez, D., Darocha, R. P., Sloan, L. C., and Steiner, A.: Regional climate modeling for the developing world, B. Am. Meteorol. Soc., 88, 1395–1409, 2007.

Pinty, B., Taberner, M., Haemmerle, V. R., Paradise, S. R., Vermote, E., Verstraete, M. M., Gobron, N., and Widlowski, J.: Global-scale comparison of MISR and MODIS land surface model, J. Climate., 24, 732–749, 2011.

Reid, J. S., Piketh, S. J., Kahn, R., Bruintjes, R. T., and Holben, B. N.: A summary of first year activities of the United Arab Emirates unified aerosol experiment: UAE^2, Naval Research Laboratory, NRL/MR/7534–05-8899, Monterey, CA, USA, 2005.

Remer, L. A., Kaufman, Y. J., Tanre, D., Mattoo, S., Chu, D. A., Martins, J. V., Li, R.-R., Ichoku, C., Levy, R. C., Kleidman, R. G., Eck, T. F., Vermote, E., and Holben, B. N.: The MODIS aerosol algorithm, products, and validation, J. Atmos. Sci., 62, 947–973, 2005.

ACPD
15, 1523–1571, 2015

Schmid, B., Michalsky, J., Halthore, R., Beauharnois, M., Harrison, L., Livingston, J., Russell, P., Holben, B., Eck, T., and Smirnov, A.: Comparison of aerosol optical depth from four solar radiometers during the fall 1997 ARM intensive observation period, Geophy. Res. Lett., 26, 2725–2728, 1999.

Shalaby, A., Zakey, A. S., Tawfik, A. B., Solmon, F., Giorgi, F., Stordal, F., Sillman, S., Zaveri, R. A., and Steiner, A. L.: Implementation and evaluation of online gas-phase chemistry within a regional climate model (RegCM-CHEM4), Geosci. Model Dev., 5, 741–760, 2012.

Shao, Y., Raupach, M. R., and Findlater, P. A.: Effect of saltation bombardment on the entrainment of dust by wind, J. Geophys. Res., 98, 12719–12726, 1993.

Shao, Y., Wyrwoll, K., Chappell, A., Huang, J., Lin, Z., Mctainsh, G. H., Mikami, M., Tanaka, T. Y., Wang, X., and Yoon, S.: Dust cycle: an emerging core theme in earth system science, Aeolian Res., 2, 181–204, 2011.

Smirnov, A., Holben, B. N., Dubovik, O., O'Neil, N. T., Eck, T. F., Westphal, D. L., Goroch, A. K., Pietras, C., and Slutsker, I.: Atmospheric aerosol optical properties in the Persian gulf, J. Atmos. Sci., 59, 620–634, 2002.

Solmon, F., Giorgi, F., and Liousse, C.: Aerosol modeling for regional climate studies: application to anthropogenic particles and evaluation over a European/African domain, Tellus B Chem. Phys. Meteorol., 58, 51–72, 2006.

Solmon, F., Mallet, M., Elguindi, N., Giorgi, F., Zakey, A., and Konare, A.: Dust aerosol impact on regional precipitation over western Africa: mechanisms and sensitivity to absorption properties, Geophys. Res. Lett., 35, L24705, doi:10.1029/2008GL035900, 2008.

Solmon, F., Elguindi, N., and Mallet, M.: Radiative and climatic effects of dust over west Africa as simulated by a regional climate model, Clim. Res., 52, 97–113, doi:10.3354/cr01039, 2012.

Stanelle, T., Vogel, B., Vogel, H., Baumer, D., and Kottmeier, C.: Feedback between dust particles and atmospheric processes over west Africa during dust episodes in March 2006 and June 2007, Atmos. Chem. Phys., 10, 10771–10788, doi:10.5194/acp-10-10771-2010, 2010.

Steiner, A. L., Tawfik, A. B., Shalaby, A., Zakey, A. S., Abdel-Wahab, M. M., Salah, Z., Solmon, F., Sillman, S., and Zaveri, R. A.: Climatological Simulations of Ozone and atmospheric aerosols in Greater Cairo region, Clim. Res., 59, 207–228, doi:10.3354/cr01211, 2014.

Stefanski, R. and Sivakumar, M. V. K.: Impact of sand and dust storms on Agriculture and potential agricultural application of a SDSWS, IOP C. Ser. Earth Env., 7, 012016, doi:10.1088/1755-1307/7/1/012016, 2009.

ACPD
15, 1523–1571, 2015

Tawfik, A. B. A., and Steiner, L.: The role of soil ice in land atmosphere coupling over the United States: a soil moisture-precipitation winter feedback mechanism, J. Geophy. Res., 116, D02113, doi:10.1029/2010JD014333, 2011.

Tegan, I. and Lacis, A. A.: Modeling of particle size distribution and its influences on the radiative properties of mineral dust aerosol, J. Geophys. Res., 101, 19237–19244, 1996.

Torres, O., Bhartia, P. K., Sinyuk, A., Welton, E. J., and Holben, B.: Total Ozone Mapping spectrometer measurements of aerosol absorption from space: comparison to SAFARI 2000 ground-based observations, J. Geophy. Res., 110, D10S18, doi:10.1029/2004JD004611, 2005.

Wilkerson, W. D.: Dust and sand forecasting in iraq and adjoining countries, Tech. Rep. AWS/TN-91/001, Air Weather Service, Scott Air Force Base, Illinois, USA, 1991.

Woodward, S.: Modeling the atmospheric life cycle and radiative impact of mineral dust in the Hadley Centre climate model, J. Geophys. Res., 106, 18155–18166, 2001.

Zakey, A. S., Solmon, F., and Giorgi, F.: Implementation and testing of a desert dust module in a regional climate model, Atmos. Chem. Phys., 6, 4687–4704, 2006, http://www.atmos-chem-phys.net/6/4687/2006/.

Zakey, A. S., Giorgi, F., and Bi, X.: Modeling of sea salt in a regional climate model: fluxes and radiative forcing, J. Geophy. Res., 113, D14221, doi:10.1029/2007JD009209, 2008.

Zhang, D. F., Zakey, A. S., Gao, X. J., Giorgi, F., and Solmon, F.: Simulation of dust aerosol and its regional feedbacks over east Asia using a regional climate model, Atmos. Chem. Phys., 9, 1095–1110, 2009, http://www.atmos-chem-phys.net/9/1095/2009/.

ACPD
15, 1523–1571, 2015

Table 1. Monthly deviation in [%] from the AOD annual average median for each site. Bold numbers indicate values with deviations of at least +20 % from the AOD annual average median and are considered dust season.

	AERO			MODIS			MISR			OMI			MODEL		
	Kuwait	SOLAR	UAE	Kuwait	SOLAR	UAE	Kuwait	SOLAR	UAE	Kuwait	SOLAR	UAE	Kuwait	SOLAR	UAE
Annual median	0.40	0.27	0.32	0.47	0.34	0.30	0.42	0.44	0.43	0.63	0.51	0.42	0.23	0.33	0.37
Jan	−51	−55	−42	−25	−33	−48	−46	−33	−37	−38	−31	−26	−42	−28	−42
Feb	−26	−26	−23	1	−8	−28	−7	−7	−32	−4	2	−11	2	−9	−23
Mar	−10	−0.3	−16	−2	2	−16	−14	−1	−17	0.3	13	−4	17	**24**	11
Apr	**25**	**23**	**22**	**44**	**56**	12	**47**	**28**	12	**38**	**29**	5	**56**	**28**	15
May	**51**	**52**	**24**	**46**	**42**	7	**65**	**33**	**31**	**23**	**30**	**20**	**26**	18	7
Jun	**47**	**38**	**37**	**38**	**36**	**53**	**39**	**48**	**33**	**37**	**23**	**41**	17	**26**	17
Jul	**40**	**23**	**52**	−2	6	**78**	**24**	7	**58**	16	17	**49**	**37**	**65**	**82**
Aug	10	**32**	**34**	−24	11	**56**	1	**20**	**55**	2.9	−1	**21**	15	**55**	**123**
Sep	−9	10	5	−25	3	−2	−17	1	−2	−3	3	−9	−25	−25	−23
Oct	−3	−15	−14	6	−27	−32	−11	−26	−31	−4	−13	−18	−41	−59	−62
Nov	−22	−34	−38	−15	−36	−37	−27	−31	−31	−30	−33	−31	−35	−52	−55
Dec	−52	−48	−41	−26	−53	−41	−53	−39	−38	−37	−39	−38	−30	−42	−50

ACPD
15, 1523–1571, 2015

Table 2. The relative error of modeled AOD, with respect to each observational dataset for each station. The first column is the modeled AOD value, the other columns are the relative errors in [%].

	Kuwait					SOLAR					UAE				
	Model	AERO	MODIS	MISR	OMI	Model	AERO	MODIS	MISR	OMI	Model	AERO	MODIS	MISR	OMI
Jan	0.13	−33.2	−61.7	−41.1	−66.1	0.23	92.7	5.4	−18.7	−32.3	0.21	14.5	37.4	−21.9	−31.5
Feb	0.23	−21.0	−50.0	−39.2	−60.7	0.30	46.0	−3.3	−26.8	−43.2	0.28	16.5	32.4	−2.9	−23.8
Mar	0.27	−26.2	−40.8	−24.9	−57.5	0.41	49.0	18.0	−5.6	−29.4	0.41	54.1	64.1	16.2	2.7
Apr	0.36	−29.4	−46.6	−42.2	−58.8	0.42	25.0	−19.7	−24.9	−35.4	0.43	8.0	25.9	−12.2	−4.1
May	0.29	−52.7	−57.4	−58.2	−62.8	0.39	−7.4	−19.3	−33.4	−41.3	0.40	−0.8	22.4	−30.2	−21.8
Jun	0.27	−55.0	−58.4	−54.0	−68.9	0.41	8.6	−10.1	−36.1	−33.9	0.44	−0.9	−5.7	−24.4	−26.8
Jul	0.31	−44.6	−30.4	−39.7	−56.7	0.54	60.3	51.3	15.6	−9.0	0.68	38.0	25.2	−1.4	7.6
Aug	0.26	−41.1	−24.1	−38.0	−59.1	0.51	41.3	36.4	−3.1	3.1	0.83	91.7	75.1	23.3	61.5
Sep	0.17	−53.3	−50.8	−50.9	−71.8	0.24	−19	−29.6	−44.9	−53.3	0.28	−15.8	−3.8	−32.8	−25.4
Oct	0.13	−65.6	−69.0	−63.9	−77.5	0.13	−43.1	−46.2	−58.8	−69.8	0.14	−49.5	−31.3	−53.1	−59.3
Nov	0.15	−52.6	−62.0	−51.3	−66.2	0.15	−14.2	−27.3	−48.1	−53.5	0.16	−18.0	−13.8	−45.3	−43.8
Dec	0.16	−18.4	−53.6	−19.9	−59.5	0.19	32.6	21.1	−28.7	−38.4	0.18	−3.4	2.5	−31.3	−29.8

ACPD
15, 1523–1571, 2015

Table 3. The annual Bottom of Atmosphere Radiative Forcing (BOARF) and the Annual Top of Atmosphere Radiative Forcing (TOARF), respectively of the AERONET and RegCM4 datasets. Average of monthly medians are shown.

	BOARF ($W m^{-2}$)		TOARF ($W m^{-2}$)	
	AERONET	RegCM4	AERONET	RegCM4
Kuwait Uni.	−65.77	−11.58	−17.20	−3.47
Solar-Village	−44.45	−13.21	−5.75	−2.91
Mezaira	−45.87	−11.43	−7.21	−3.62
Average	−52.03	−12.07	−10.05	−3.33

ACPD
15, 1523–1571, 2015

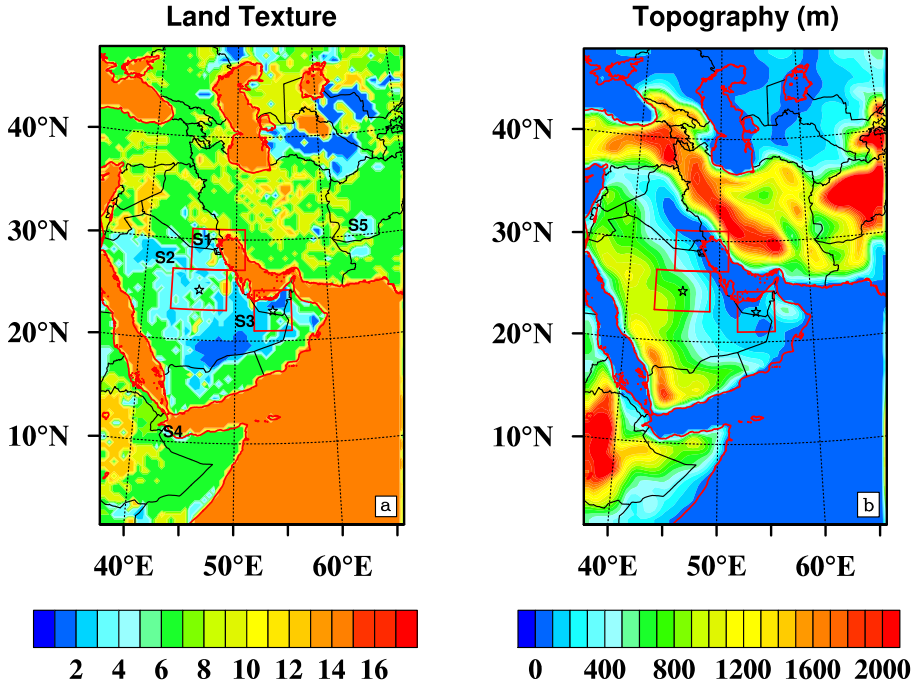

Figure 1. (a) The BATS land texture categories; **(b)** the topography height in meter. Stars indicate the location of the AERONET stations. All area average calculations are done for the areas surrounded by red rectangles. For detailed description of the BATS land texture categories see Zakey et al. (2006).

ACPD
15, 1523–1571, 2015

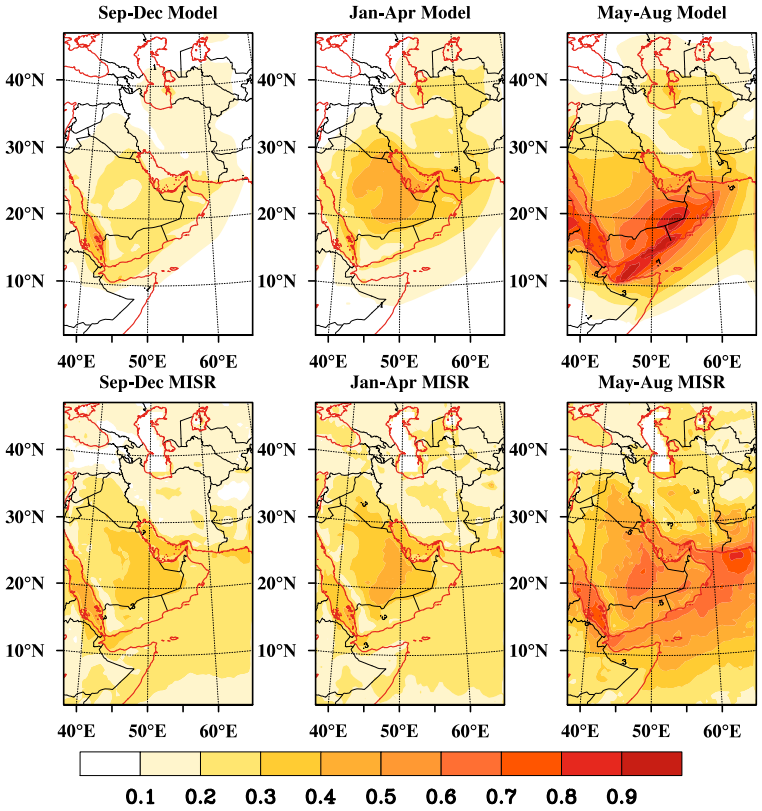

Figure 2. AOD seasonal average of 13 year of RegCM4 simulation versus MISR observations. For each season the upper panels show modeled AOD and the lower panels show MISR's observed AOD. The legend indicates the AOD.

ACPD
15, 1523–1571, 2015

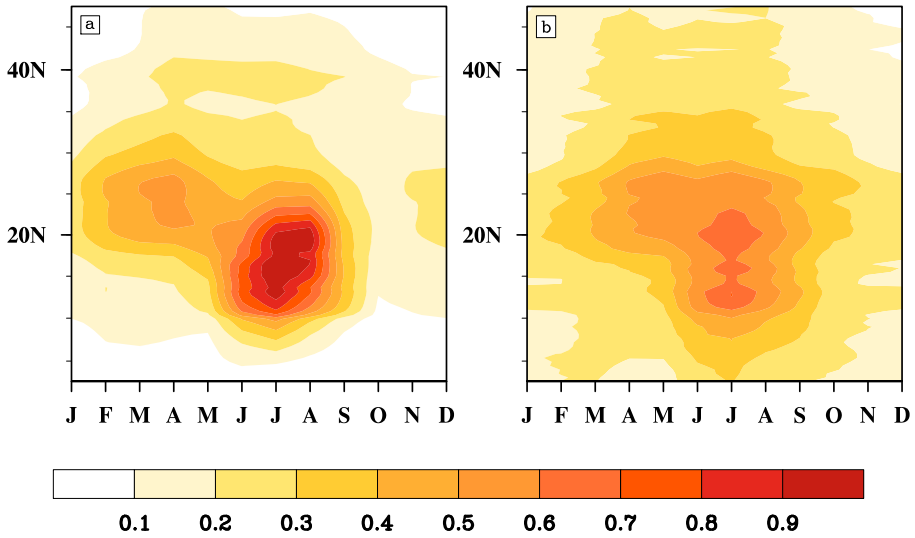

Figure 3. The annual cycle of the zonally averaged AOD (averaged from 44 to 56° E and over the 13 year simulation period), **(a)** RegCM4.4 AOD, **(b)** MISR AOD.

ACPD
15, 1523–1571, 2015

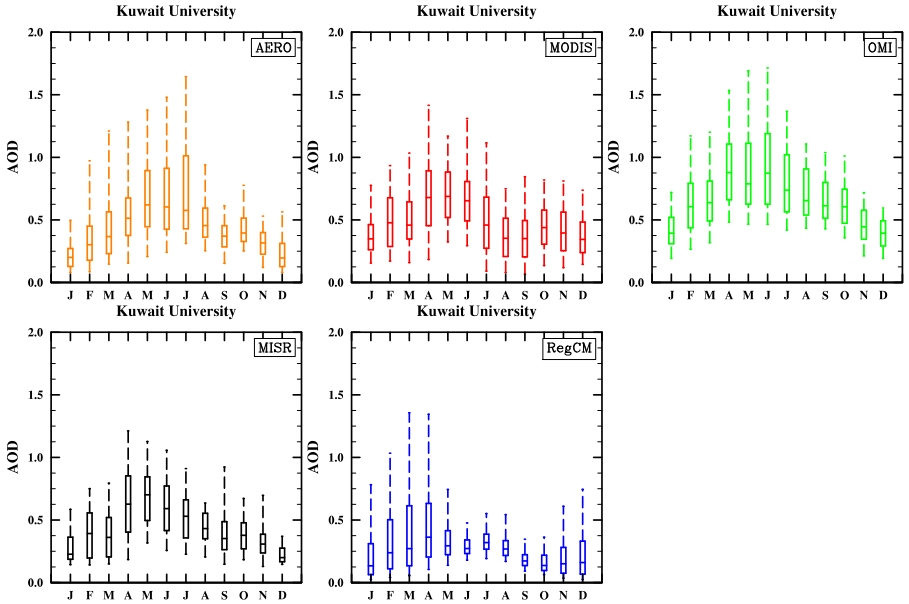

Figure 4. The AOD annual cycle statistics (5 percentile, 20 percentile, median, 75 percentile, 95 percentile) of AERONET, MODIS (deep-blue), OMI, MISR and RegCM for Kuwait University site, Kuwait.

ACPD
15, 1523–1571, 2015

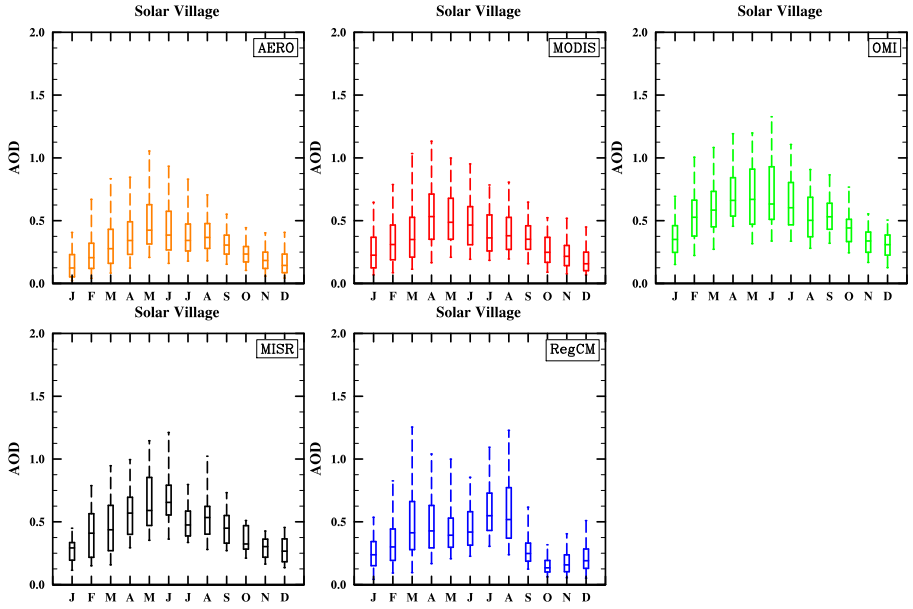

Figure 5. The AOD annual cycle statistics as in Fig. 4 but for Solar-Village site, Saudi Arabia.

ACPD
15, 1523–1571, 2015

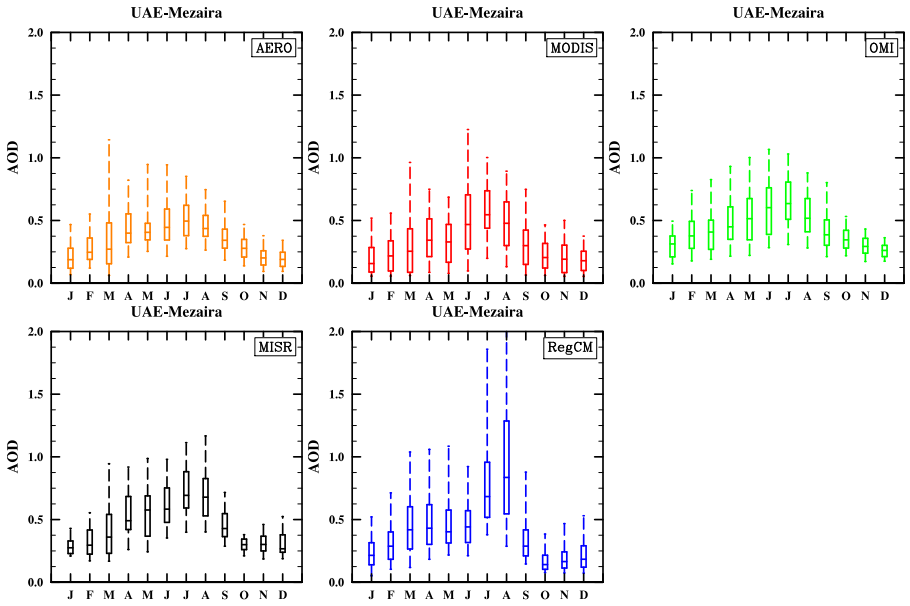

Figure 6. The AOD annual cycle statistics as in Fig. 4 but for Mezaira (UAE) site.

ACPD
15, 1523–1571, 2015

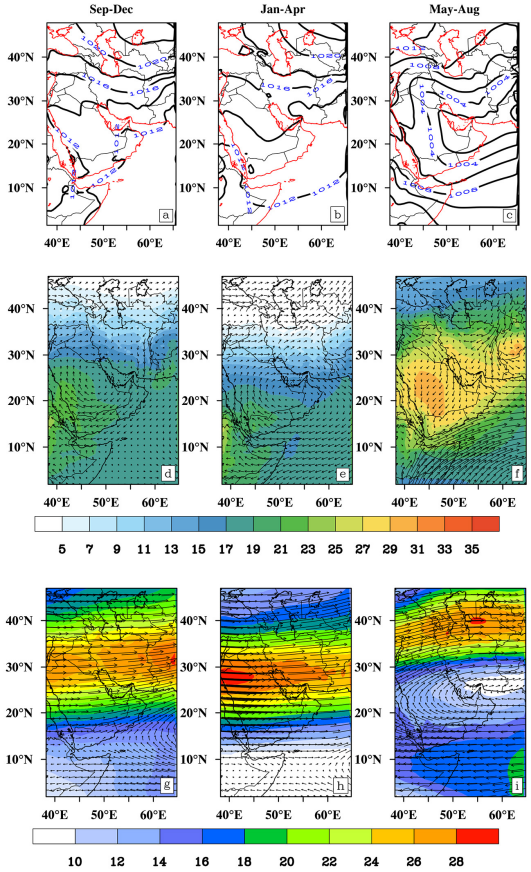

Figure 7. (a–c) The climatology (seasonal average) of the modeled mean sea level pressure in hPa, **(d–f)** the modeled 850 hPa Temperature in ˚C (shaded colors) and wind field (represented by vectors), **(g–h)** the modeled 200 hPa wind speed in ms^{-1} (shaded colors) and wind field (represented by vectors). All data is based on the 2000–2012 time interval.

ACPD
15, 1523–1571, 2015

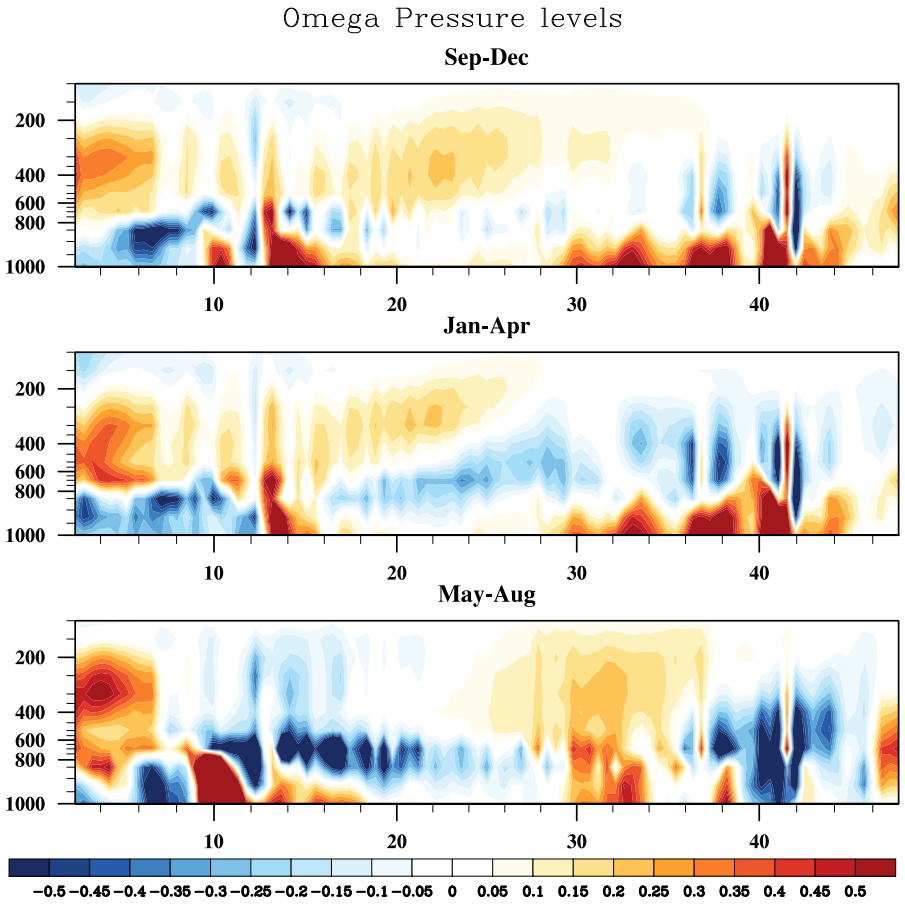

Figure 8. Climatology (seasonal average) of vertical velocity zonally averaged (averaged from 36 to 45° E and based on 2000–2012 time interval). The color scale represents vertical velocity in hPa s^{-1}. The *x* axis is latitude and *y* axis is pressure level in hPa.

ACPD
15, 1523–1571, 2015

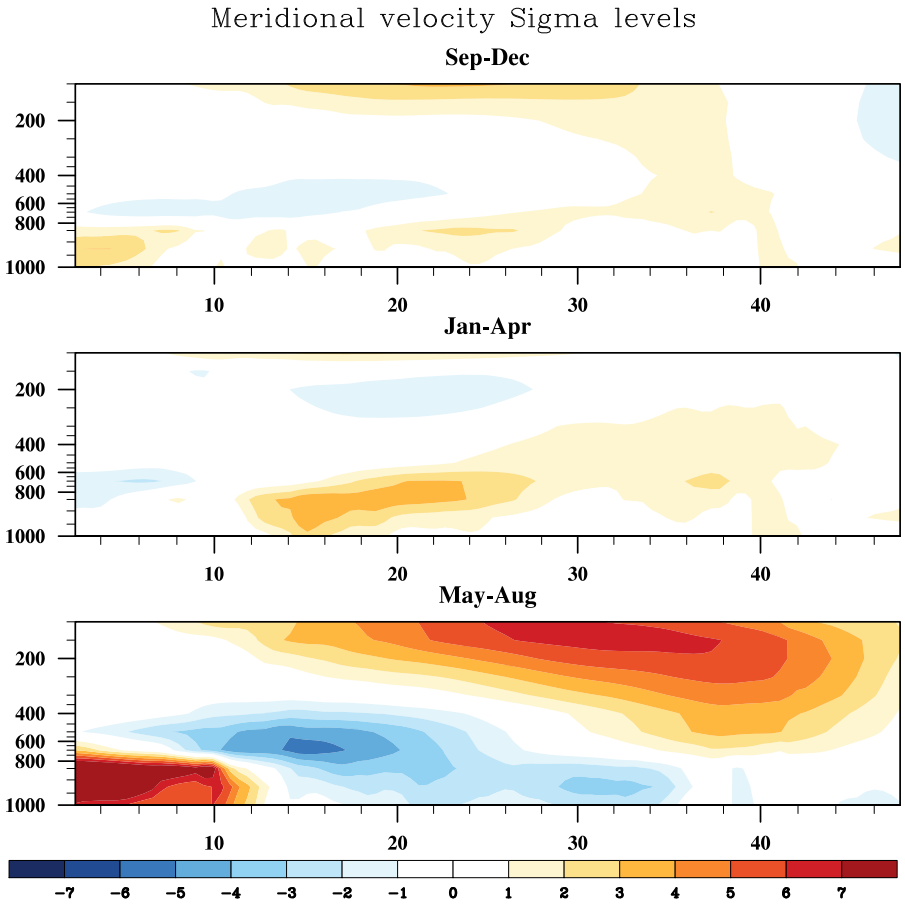

Figure 9. Climatology (seasonal average) of meridional velocity zonally averaged (averaged from 36 to 50° E and based on 2000–2012 time interval). The color scale represents velocity in ms^{-1}. The *x* axis is latitude and *y* axis is pressure level in hPa.

ACPD
15, 1523–1571, 2015

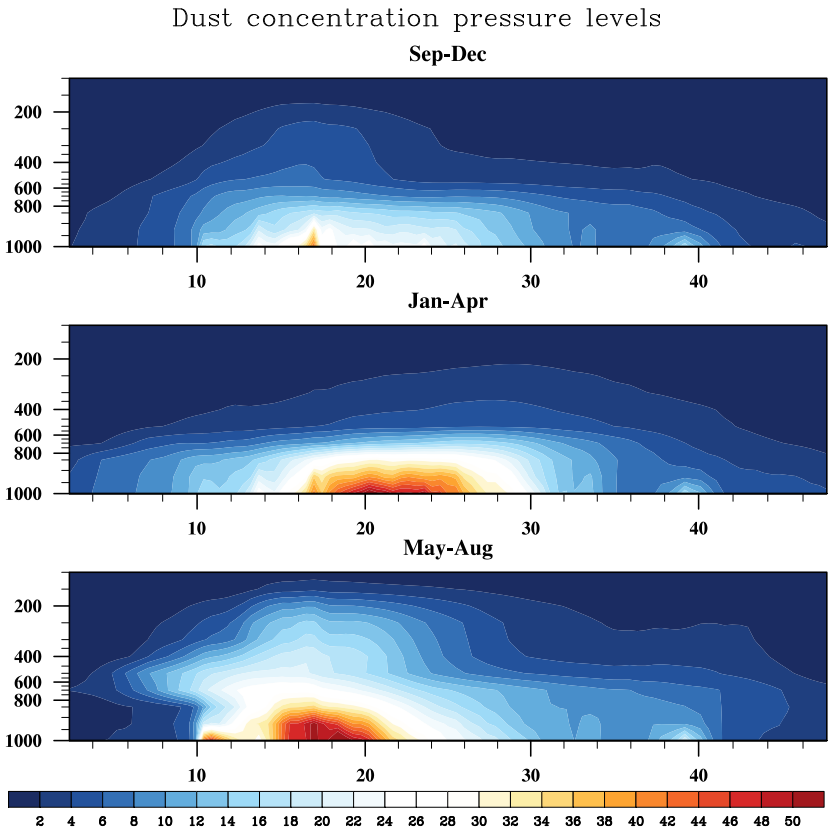

Figure 10. Climatology (seasonal average) of fine dust (0.01–1 µm) concentration in ($\mu g\,m^{-3}$) zonally averaged (averaged from 36 to 50° E and based on 2000–2012 time interval). The color scale represents concentration in $\mu g\,m^{-3}$. The *x* axis is latitude and *y* axis is pressure level in hPa.

ACPD
15, 1523–1571, 2015

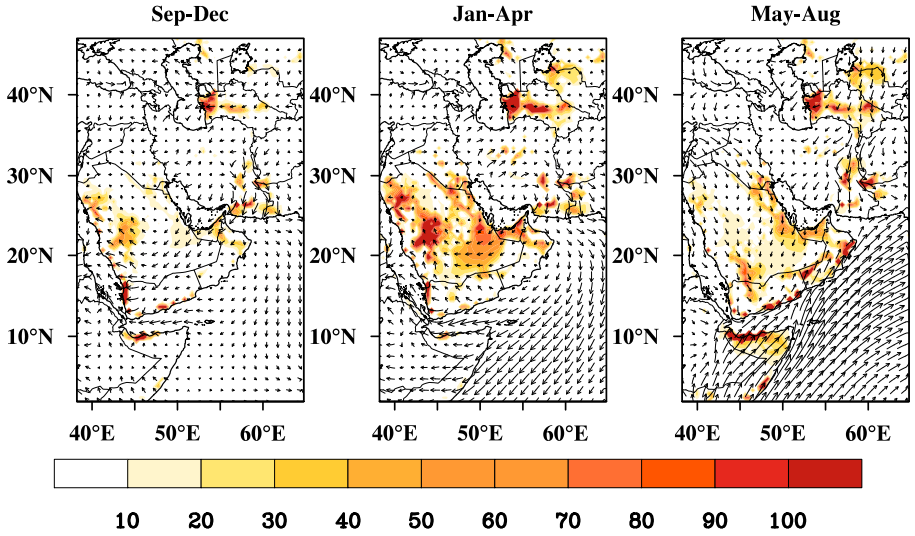

Figure 11. Climatology (seasonal average) of surface fine (0.01–1 µm) dust emission flux for fine dust (mg m^{-2} day^{-1}) based on 2000–2012 interval.

ACPD
15, 1523–1571, 2015

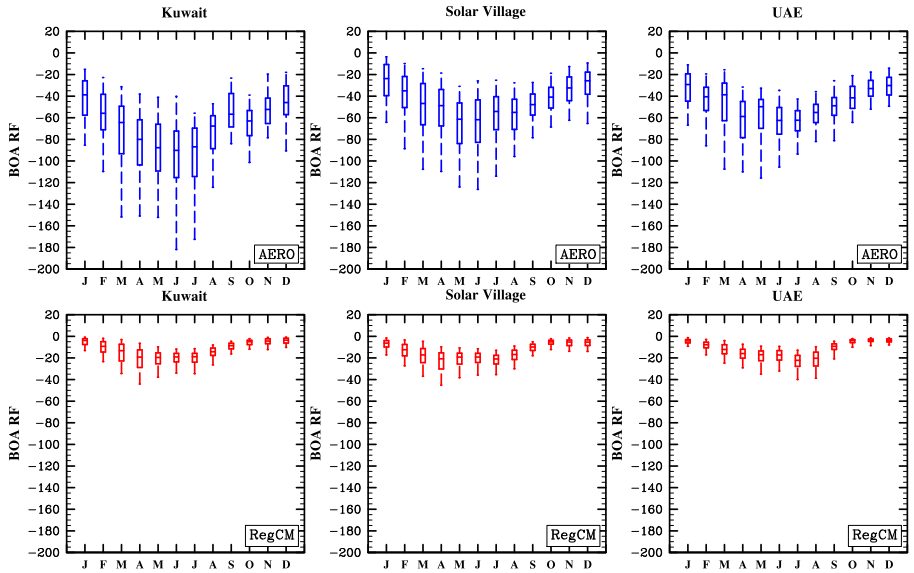

Figure 12. The Bottom of Atmosphere radiative forcing of (BOARF) AERONET inversion products (blue) and the RegCM4 output (red), spatially averaged around the AERONET sites.

ACPD
15, 1523–1571, 2015

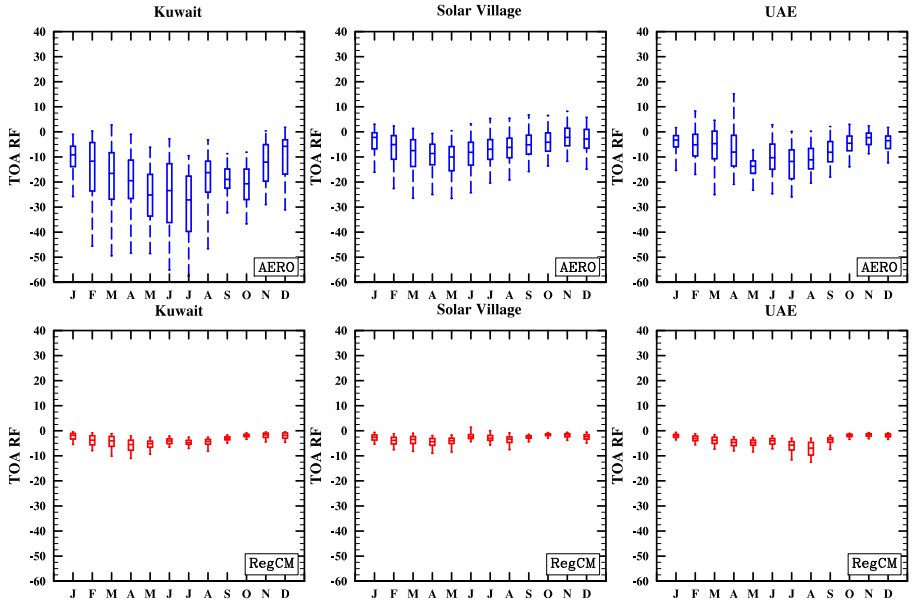

Figure 13. The Top of Atmosphere radiative forcing (TOARF) of AERONET inversion products (blue) and the RegCM4 output (red), spatially averaged around the AERONET sites.

ACPD
15, 1523–1571, 2015